



International Communications in Heat and Mass Transfer

journal homepage: www.elsevier.com/locate/ichmt**Molecular dynamics study of water vapor condensation on a composite wedge-shaped surface with multi wettability gradients**Bo Xu^{a,b,c}, Zhenqian Chen^{a,b,c,*}^a School of Energy and Environment, Southeast University, Nanjing, PR China^b Jiangsu Provincial Key Laboratory of Solar Energy Science and Technology, School of Energy and Environment, Southeast University, Nanjing, PR China^c Key Laboratory of Energy Thermal Conversion and Control of Ministry of Education, School of Energy and Environment, Southeast University, Nanjing, PR China

ARTICLE INFO

Keywords:

FWC
DWC
Composite wedge-shaped surface
Multi wettability gradients
Vertex angle

ABSTRACT

To find out whether the composite wedge-shaped surface with multi wettability gradients could accelerate the condensate drainage in a micro view, the model of water vapor condensation on such surface was built and studied by molecular dynamics (MD). The vertex angle and wettability gradient of wedge-shaped surface were investigated to obtain the best condition for accelerated removal of condensate. The wettability gradient of two surfaces was divided into three groups: Group A (hydrophilic - super hydrophilic), Group B (hydrophobic - hydrophilic) and Group C (hydrophobic - super hydrophobic). The vertex angle was changed from 7°, 10°, 14° to 20°. Filmwise condensation (FWC) appeared in Group A and dropwise condensation (DWC) formed in Group B. However, there was no condensation in Group C. Although the FWC in Group A could drain, the drainage rate was slow. Only in Group B, the DWC could form water droplet and the movement of droplet could be controlled by the wedge-shaped surface, which was helpful for condensate drainage. When comparing the effect of different vertex angle, the smaller vertex angle could finish the FWC more quickly in Group A due to the smaller area of the super hydrophilic surface. In group B, small wedge-shaped surface would take more time to form main nuclei, while large wedge-shaped surface forming two nuclei also took more time to form a whole nanoscale droplet. In that case, DWC rate was quicker and condensation drainage was better in vertex angle of 14° in these four conditions.

1. Introduction

Many organisms possess special surface structures with unique wettability and shapes for water collection. For example, certain beetles collect drinking water from fog via their textured backs with alternating hydrophilic and hydrophobic regions [1]. Due to the directional droplet transportation caused by Laplace pressure and wettability gradients [2], conical cactus spines [3] and spindle-shaped spider silk [4,5] exhibit efficient water collection from the fog. Controlled self-propelling of droplet has an extensive application prospect in many fields [6–8], such as fog-harvesting, microfluidic device, condensing apparatus and industrial filtration equipment.

Either dropwise condensation (DWC) or filmwise condensation (FWC) will appear conventionally about vapor condensation on a cold surface. What's more, it has been confirmed that DWC could produce an order of magnitude higher than FWC in heat transfer coefficient [10–13]. In addition, the condensation mode mainly depends on the surface wettability. Although some scholars have studied the effect of

surface wettability to form DWC in microscale, while the movement of condensation droplet was uncontrolled. Therefore, it is particularly meaningful [14–20] to design a stable and controlled surface which enables DWC for condensate drainage.

With the rapid development of computational capabilities, molecular dynamics (MD) simulation has been widely used to explore the microscopic interactions, including vapor condensation. The concept of molecular clustering has been introduced to explain the formation mechanism of initial droplets [21] and the nucleation process has been investigated using MD simulation [22–28]. For example, Yasuoka used MD simulation to investigate the dynamics of vapor phase homogeneous nucleation at the triple point temperature under supersaturation ratio 6.8 for a Lennard-Jones fluid [22] and at 350 K under supersaturation ratio 7.3 for the vapor phase of water [23]. It was found the kinetically defined critical nucleus size, at which the growth and decay rates are balanced, is 30–40 for Lennard-Jones fluid and 30–45 for water. Jung [24] focused on the formation and growth of nanoscale droplets inside polymer networks by MD simulation and concluded that

* Corresponding author at: School of Energy and Environment, Southeast University, Nanjing, PR China.

E-mail address: zqchen@seu.edu.cn (Z. Chen).

droplet growth beyond the initial nucleation stage occurs by different mechanisms depending on the mesh size: droplets grow mainly by diffusion and coalescence inside polymer networks with large mesh sizes (as observed in bulk), whereas Ostwald ripening becomes a more dominant mechanism for droplet growth for small mesh sizes. Niu [29] found that FWC caused more efficient heat transfer than DWC in macroscale because of a lower interfacial thermal resistance between condensed water and hydrophilic surface. Xu [30] studied heterogeneous nucleation of water droplet on surfaces and concluded that formation and growth rate of nuclei increased with solid-liquid interaction intensities. Sheng [31] observed the different condensation modes (no-condensation, DWC and FWC) and analyzed their characteristics quantitatively by temporal profiles of surface clusters. Therefore, MD was quite suitable to study the mechanism and behavior of condensation on a controlled surface with multi wettability gradients in microscale.

Here, the vertex angle and wettability gradients of composite wedge-shaped surface on water condensation were studied by MD to find out whether such a surface could accelerate the condensate drainage in a micro view.

2. Models and methods

All of molecular dynamics simulations are carried out by LAMMPS package [32]. To investigate the wettability of solid surface, the initial water model including 2830 water molecules is put on copper-type surface as shown in Fig. 1(a). The TIP3P water model [33] was employed containing a single Lennard-Jones center. Water molecule had three charges, including $-0.834e$ for oxygen atom and $+0.417e$ for hydrogen atoms with an angle of 104.52° between oxygen and hydrogen atoms. A rigid-body water model was regarded by Shake algorithm to fix the angle and bond distance of water model. The ϵ_{o-o} and σ_{o-o} in water molecule are 0.1521 kcal/mol and 3.1507 \AA respectively. The atoms of copper-type surface are fixed to their lattice sites, providing a realistic model of the solid surface [34]. The initial water model will evolve into a sphere droplet with different contact angles representing surface wettability.

The model of water condensation containing 8882 water molecules and 52,354 copper-type atoms was built in Fig. 1(b) to study the effect of vertex angle (α) and wettability gradients of wedge-shaped surface by non-equilibrium molecular dynamics (NEMD) simulations. The vertex angle was changed from 7° , 10° , 14° to 20° . As is well known, contact angle (θ) of droplet could represent the wettability of solid surface. The wettability of purple copper atoms and green copper atoms were changed in three groups: Group A (hydrophilic ($\theta_1 = 70^\circ$) - super hydrophilic ($\theta_2 = 20^\circ$)), Group B (hydrophobic ($\theta_3 = 120^\circ$) - hydrophilic ($\theta_4 = 70^\circ$)) and Group C (super hydrophobic ($\theta_5 = 150^\circ$) -

hydrophobic ($\theta_6 = 120^\circ$)). The liquid film concentrating on hot wall was treated as a vapor source before condensation happened. Several layers of copper-type atoms were built as the cold and hot wall. The outside two layers were fixed to make sure the solid wall wouldn't break apart and next two layers were regarded as heating or cooling source. Finally, the inside two layers were used to exchange energy between water molecules and hot or cold walls. The method to build the heating or cooling model was used in many studies [35–37] and had been proved to avoid artificial thermal resistance effectively [38]. Therefore, the interaction between water molecules and composite wedge-shaped surface were changed to simulate condensation with different vertex angles and wettability gradients.

All simulations were carried out in two stages with a time step of 2 fs. It took 100 ps for first stage and 2000 ps for second stage. In the first stage, the NVT ensemble with a Nose-Hoover thermostat at 298 K was adopted until the water system reached equilibrium of two phases between vapor and liquid. In the second stage, the water equilibrium system was taken as the initial configuration. The thermostat adopted on copper atoms of lower surface and water molecules was removed to create a temperature difference and NVE ensemble was applied on water system and copper atoms of lower surface. The temperature of hot wall increased to 498 K while cold wall was maintained at 298 K. The water vapor of hot wall with high temperature began to evaporate and then condensed on the cold surface. In the whole simulation, the long-range electrostatic interactions were calculated by PPPM (particle-particle particle-mesh) method. The periodic boundary condition was applied in all three spatial dimensions of the simulation box. Verlet algorithm was used on Newton's motion equation numerically.

The interaction between copper-type surface and water molecules is also assumed to be 12–6 Lennard-Jones (LJ) particles [39] as followed:

$$U_{ij}(r_{ij}) = 4\epsilon_{ij} \left[\left(\frac{\sigma_{ij}}{r_{ij}} \right)^{12} - \left(\frac{\sigma_{ij}}{r_{ij}} \right)^6 \right] \quad (1)$$

where r_{ij} , ϵ_{ij} and σ_{ij} are the distance, well depth and equilibrium distance between a pair of atoms or charges. ϵ_{cu-o} can be used to tune the wettability of the copper-type surface. ϵ_{ij} and σ_{ij} between different species i and j are calculated by using Lorentz-Bertholet mixing rule

$$\epsilon_{ij} = \sqrt{\epsilon_i \epsilon_j} \quad (2)$$

$$\sigma_{ij} = \frac{(\sigma_i + \sigma_j)}{2} \quad (3)$$

The cutoff distances for LJ and Coulomb interactions are 10 \AA and 12 \AA .

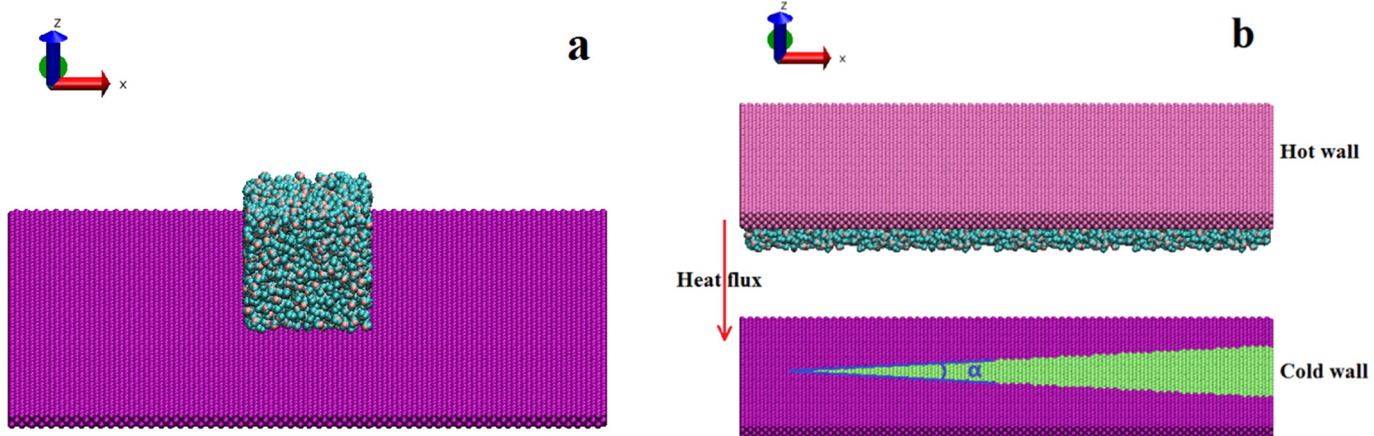


Fig. 1. (a) Initial water model on copper-type surface; (b) Model of water condensation in a composite wedge-shaped surface.

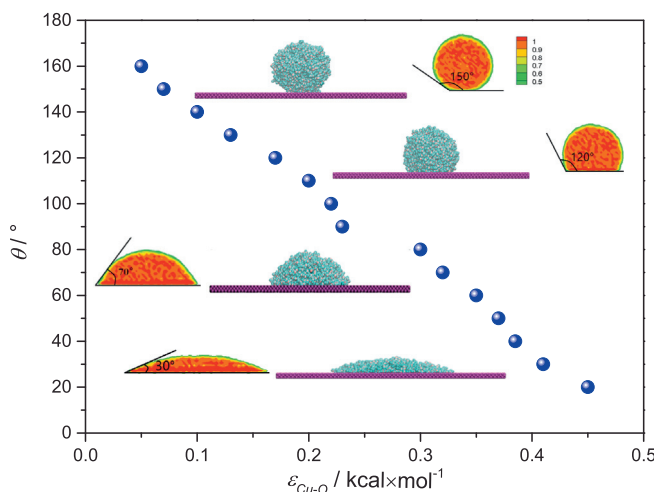


Fig. 2. Correlations of contact angle (θ) with ε_{Cu-O} .

3. Results and discussion

3.1. Static state

As mentioned above, ε_{Cu-O} was used to tune the wettability of copper-type surface. To study the water condensation in different wettability surface, the relationships between ε_{Cu-O} and contact angles of water droplet should be measured firstly. Water droplet on the smooth copper-type surface with different ε_{Cu-O} was simulated. The correlations of contact angle with ε_{Cu-O} and some density profiles were depicted in Fig. 2. The particle density on the edge of droplet was 0.5 [40].

3.2. Different wettability gradients

Clusters formation and nuclei generation were usually the initial two stages of condensation. Based on Stillinger's definition [41], any two molecules separated by less than a certain bonding distance were regarded to belong to a cluster. The size of a cluster was measured and the number of molecules of a cluster on the copper-type surface larger than 10 [31] was defined as an s-cluster (short for surface cluster). With the growth of s-cluster, it was defined as a nuclei when number of molecules of s-cluster was larger than 45 [23]. Finally, nanoscale droplet (molecules larger than 768) [42] or liquid film emerged.

The wettability of cold surface was the only thing changed during the heat transfer process. Therefore, the effect of surface wettability on condensation should be studied as the main factor in microscale. In order to investigate the water condensation mode on a composite wedge-shaped surface in different wettability gradients, transient snapshots (300 ps, 500 ps, 1000 ps, 1500 ps and 2000 ps) of three groups of vertex angle 10° were shown in Fig. 3.

Water condensation on the surface from hydrophilic to super hydrophilic was depicted in Fig. 3 a1–a5. As was well known, the super hydrophilic surface had a larger attraction to water molecules than hydrophilic surface. Hence, more s-clusters deposited discretely and some quickly formed into nuclei on the super hydrophilic surface in Fig. 3-a1. What's more, as the super hydrophilic surface was smooth, there was no special liquid core for water condensation. Consequently, the s-clusters appeared discretely. With the time went on, number and size of s-clusters and nuclei increased quickly and coalesced into each other. Most of the s-clusters and nuclei were connected on super hydrophilic surface in Fig. 3-a2, indicating a film-like condensation due to the large wettability of surface. Then, water molecules condensed continuously and some s-clusters on hydrophilic surface migrated and coalesced with existing film-like condensation, leading to that the film

continued to grow thicker (see Fig. 3 a2–a5 and Supplementary Video A). As no condensate film rupturing was observed, a FWC was identified.

Water condensation on the surface from hydrophobic to hydrophilic was described in Fig. 3 b1–b5. Nearly no s-clusters formed on the hydrophilic or hydrophobic surface in Fig. 3-b1, which means the condensation was slower than it in case of Group A. Some s-clusters formed discretely and a nucleus emerged because one s-cluster became large enough to overcome free energy barrier of nucleation on hydrophilic surface (Fig. 3-b2). Then they were able to migrate and coalesce with other clusters. The nuclei continued growing up towards nanoscale droplets and a new s-cluster became a nucleus while others downsized and failed. As can be seen from Fig. 3-b3, the nucleus on the top side of wedge-shaped surface moved towards the bottom with the action of two sides of wedge-shaped surface and it integrated into the nanoscale droplet at the bottom. After numerous coalescences, only one nanoscale droplet was observed (Fig. 3-b4) and no film-like condensation formed in this case. This nanoscale droplet continued growing up by gobbling up other molecules and clusters nearby (Fig. 3-b5). The results showed the growth of droplet was via three stages, including s-cluster formation, nuclei generation and finally nanoscale droplets emergence (see Supplementary Video B). Dropwise condensation happened in this situation. What's more, the movement of water nanoscale droplet was towards the bottom of wedge-shaped surface, indicating the controllability of condensate drainage.

On the surface from super hydrophobic to hydrophilic, as shown in Fig. 3 c1–c5, no condensation occurred. The energy barrier for nucleation on hydrophobic surface was higher, resulting in slower nucleation rate. What's more, the weak attraction of hydrophobic surface atoms to water molecules led to the departure of formed clusters from the surface. Therefore, few s-clusters appeared on hydrophobic surface (Fig. 3-c3) and no nuclei emerged (Fig. 3-c5), indicating that no s-cluster evolved into a nanoscale droplet (see Supplementary Video C). In this case, water molecules couldn't condensate on a small wettability surface.

When simulation time was 300 ps, water s-cluster and nuclei only formed in Group A and nearly no s-cluster formed in Group B and Group C. When time came to 500 ps, water s-clusters began to appear in Group B and the super hydrophilic surface in Group A was filled with s-clusters which formed a liquid film. However, there were only a few small s-clusters in Group C. With time went on, three different simulation results happened in three cases. Finally, the FWC formed in group A and DWC appeared in Group B. No condensation happened in Group C.

Condensation numbers of water molecules on copper-type surface were monitored, shown in Fig. 4(a). The condensate drainage numbers was defined by the numbers of condensed water molecules on copper-type surface touching the vertical plane of bottom of wedge-shaped surface (y - z plane, biggest x distance), described in Fig. 4(b). The condensation numbers and condensate drainage numbers of Group C were nearly 0, indication the unsuitable for water condensate drainage. As the hydrophilic surface attracted the water molecules, the condensation numbers of Group A was larger than it of Group B. However, the condensate drainage numbers was more important to judge the useful drainage. Therefore, although the FWC in Group A could drain, the drainage rate was very slow. Only in Group B, the DWC could form the water nanoscale droplet and the movement of droplet could be controlled by the wedge-shaped surface, which was helpful to condensate drainage.

3.3. Different vertex angle of wedge-shaped surface

The wettability gradient area of wedge-shaped surface could affect the condensation rate and condensate drainage. Therefore, in order to obtain the best condition for condensate drainage, three different vertex angles of 7°, 10° to 14° were studied in Group A and four different vertex angles of 7°, 10°, 14° to 20° were studied in Group B. As the

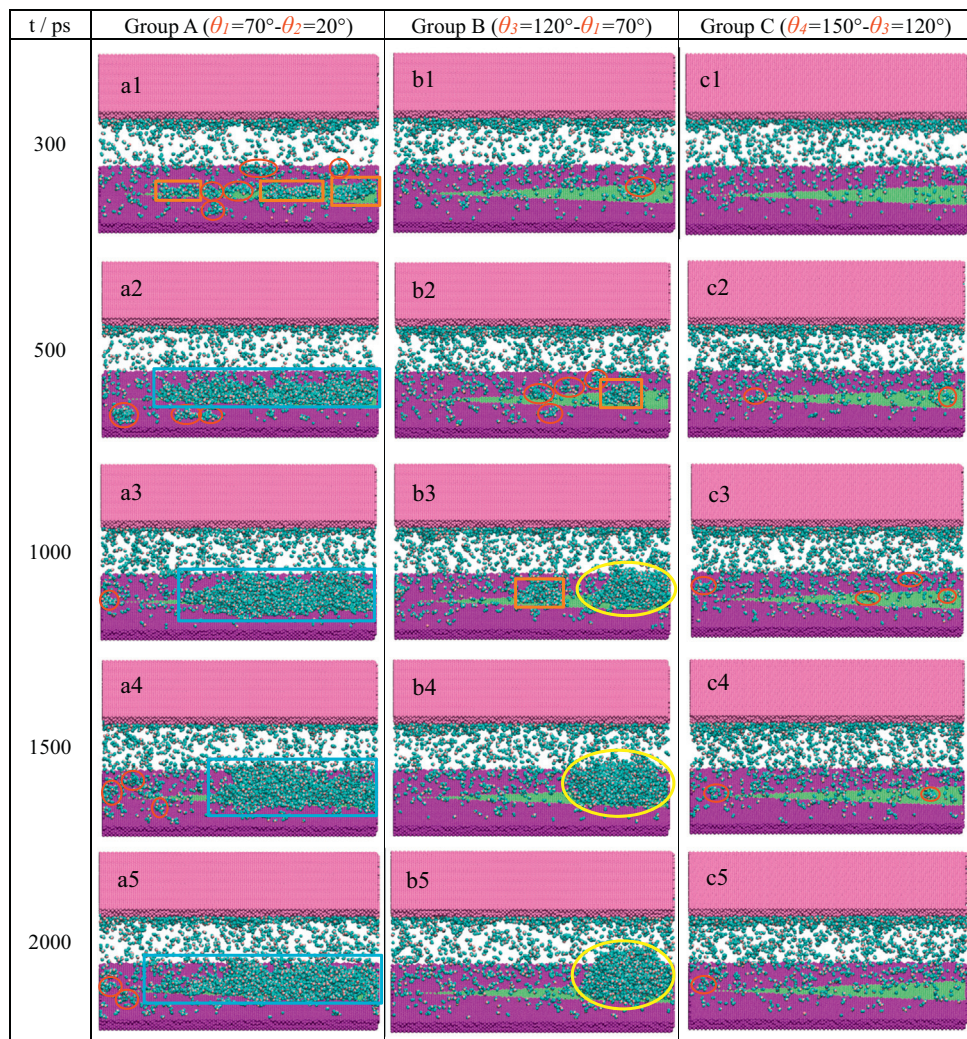


Fig. 3. Transient snapshots of water condensation in different wettability gradients (“○” represents s-cluster; “□” represents nuclei; “■” represents condensed film; “○” represents nanoscale droplet)

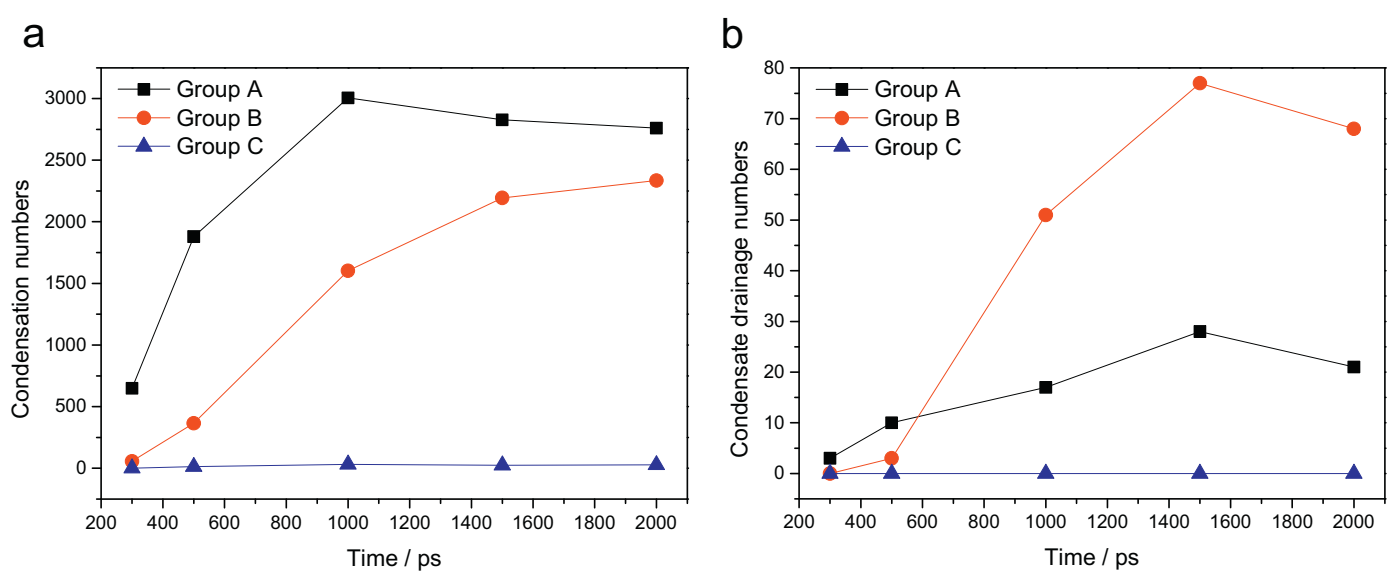


Fig. 4. Condensation numbers and condensate drainage numbers of water molecules in different groups

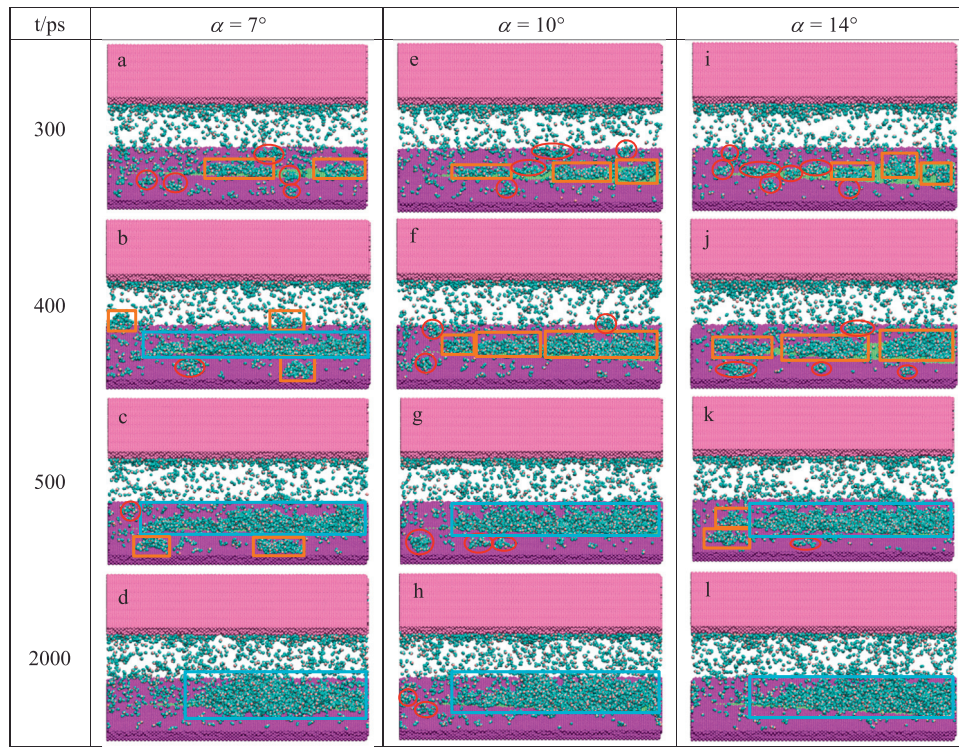


Fig. 5. Transient snapshots of condensation in different vertex angles of Group A (“○” represents s-cluster; “□” represents nuclei; “□” represents condensed film)

condensation didn't happen in Group C no matter how vertex angles changed, the result in this case would not discuss. The results of different vertex angles in Group A and Group B were discussed separately.

3.3.1. Group A ($\theta_1 = 70^\circ - \theta_2 = 20^\circ$)

The transient snapshots (300 ps, 400 ps, 500 ps and 2000 ps) of three different vertex angles in Group A were shown in Fig. 5. As the hydrophilicity of surface in Group A, the FWC happened in all cases no matter how vertex angles changed. When it was 300 ps, s-clusters and nuclei occupied more area of super hydrophilic surface in $\alpha = 10^\circ$ (Fig. 5e) than other two cases. However, when the time came to 400 ps, the super hydrophilic surface was filled with water s-clusters to form a film-like condensation and more s-clusters and nuclei began to form on hydrophilic surface in $\alpha = 7^\circ$ (Fig. 5b). Although the water s-clusters occupied more area in super hydrophilic surface in $\alpha = 10^\circ$ (Fig. 5f) than it in $\alpha = 14^\circ$ (Fig. 5j), part of super hydrophilic surface in $\alpha = 10^\circ$ was still empty showing the unfinished FWC. It indicated that the FWC was firstly finished in $\alpha = 7^\circ$ because the smallest area of super hydrophilic surface. What's more, the water s-clusters formed discretely caused the phenomena appeared at 300 ps. When time increased to 500 ps, the old s-clusters and nuclei formed in hydrophilic surface in Fig. 5c coalesced and increased the height of condensate film and new s-clusters formed again in hydrophilic surface. The same phenomena happened both in Fig. 5g and Fig. 5k. In addition, FWC was finished both in these two cases, which was slower than it in $\alpha = 7^\circ$. With the time went on, some water molecules condensed directly to condensate film. At the same time, some formed s-clusters and nuclei and then coalesced to condensate film. Finally, both two ways were to extend and increase the condensate film.

In a composite wedge-shaped surface, the smaller vertex angle could finish the FWC more quickly in Group A due to the smaller area of super hydrophilic surface. The difference of condensation numbers and condensate drainage numbers of water molecules with different vertex angles in Group A were not obvious, described in Table 1. Hence, as the FWC was not as good as DWC for condensate drainage which was discussed above, more attention should be focused on the DWC of Group B with different vertex angles.

Table 1

Condensation numbers and condensate drainage numbers of water molecules at different vertex angles of Group A.

Time/ps	$\alpha = 7^\circ$	$\alpha = 10^\circ$	$\alpha = 14^\circ$
Condensation numbers			
300	457	648	594
400	1216	1314	1330
500	1882	1880	1995
2000	2705	2760	2640
Condensate drainage numbers			
300	5	3	10
400	12	15	5
500	9	10	16
2000	13	21	25

3.3.2. Group B ($\theta_3 = 120^\circ - \theta_1 = 70^\circ$)

The transient snapshots (300 ps, 400 ps, 500 ps, 1000 ps, 1500 ps and 2000 ps) of four different vertex angles in Group B were shown in Fig. 6. In order to depict the changing process of nanoscale droplet shape clearly, the height (z-direction), width (y-direction) and length (x-direction) of the condensate nanoscale droplet at bottom of wedge-shaped surface were described in Fig. 7. \emptyset and γ were defined as follows:

$$\emptyset = \frac{\text{Height}}{\text{Length}}, \gamma = \frac{\text{Width}}{\text{Length}} \quad (4)$$

where, \emptyset and γ were used to describe the flat extent and narrow extent of droplet.

More s-clusters formed on hydrophilic surface at 300 ps in $\alpha = 20^\circ$ (Fig. 6s) and a nucleus emerged in $\alpha = 14^\circ$ (Fig. 6m). It was because the larger hydrophilic surface area provided more chances and more sites for water molecules to condense. When time came to 400 ps, two nuclei appeared on hydrophilic surface in $\alpha = 7^\circ$ (Fig. 6b) and a larger nucleus due to the larger hydrophilic surface area in $\alpha = 10^\circ$ (Fig. 6h). However, several nuclei formed in $\alpha = 14^\circ$ (Fig. 6n) and $\alpha = 20^\circ$ (Fig. 6t) and they didn't have enough time to migrate and coalesce to a larger

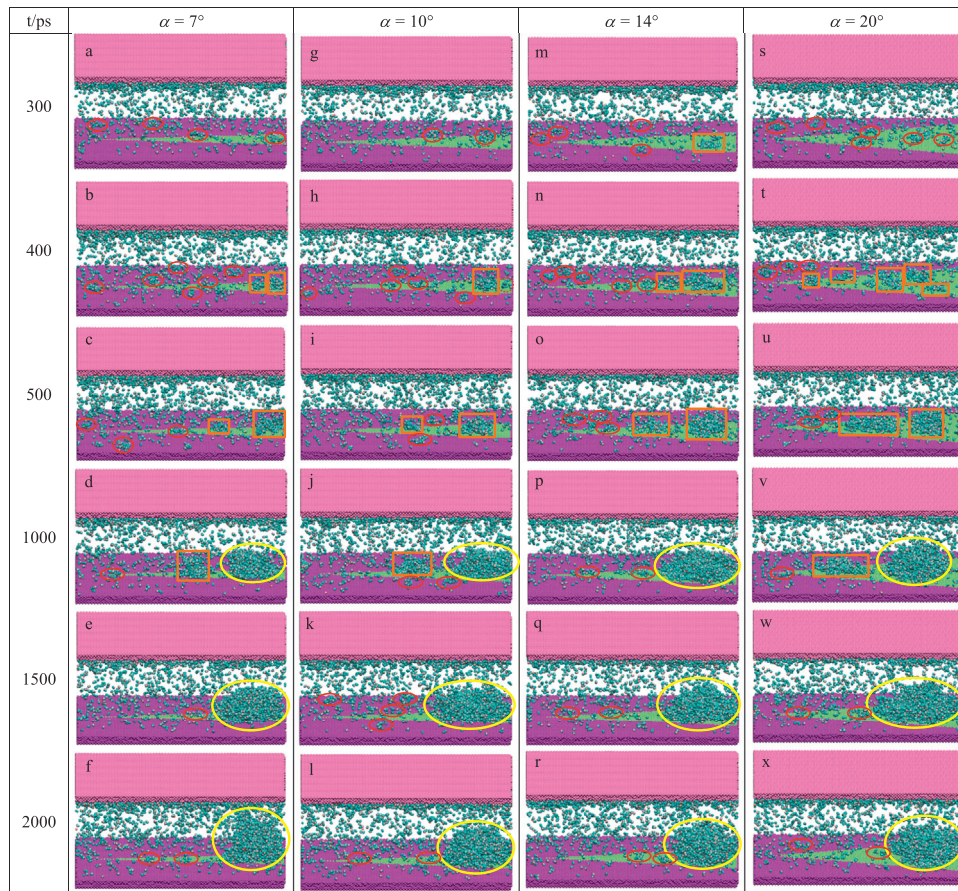


Fig. 6. Transient snapshots of condensation in different vertex angles of Group B (“○” represents s-cluster; “□” represents nuclei; “○” represents nanoscale droplet)

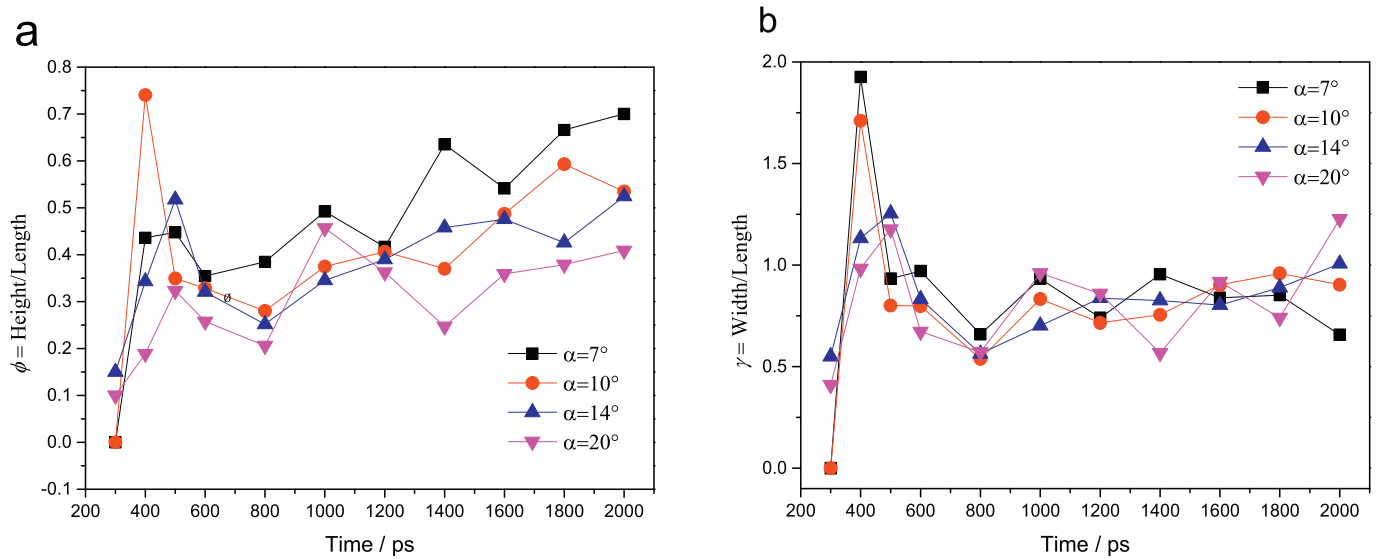


Fig. 7. The two parameters of droplet at different vertex angles of Group B

nuclei, which caused the smaller ϕ and γ than them in $\alpha = 7^\circ$ and $\alpha = 10^\circ$. At 500 ps, two separate nuclei formed apparently in all four conditions. The nucleus at the bottom of wedge-shaped surface in $\alpha = 14^\circ$ (Fig. 6o) was larger than that at the same position of other three cases (Fig. 6c, i and u), which was corresponded well with results in Fig. 7. However, the nucleus at the middle of wedge-shaped surface in $\alpha = 20^\circ$ was largest, indicating that two nuclei with similar size or significance appeared and it will take more time for two nuclei to grow and coalesce to each other to finally finish DWC in this case. As

expected, when time was 1000 ps, one nucleus still existed and the other one enlarged to a nanoscale droplet in $\alpha = 7^\circ$ (Fig. 6d), $\alpha = 10^\circ$ (Fig. 6j) and $\alpha = 20^\circ$ (Fig. 6v). The nucleus and nanoscale droplet didn't coalesce to each other because the interaction between them was not large enough to coalesce to a larger nanoscale droplet. The interaction was closely related to the size of nuclei and the distance between nuclei. When the size of nuclei was large enough and the distance between nuclei was close to each other, the interaction would be large enough to coalesce. While in these three cases, nucleus and nanoscale droplet still

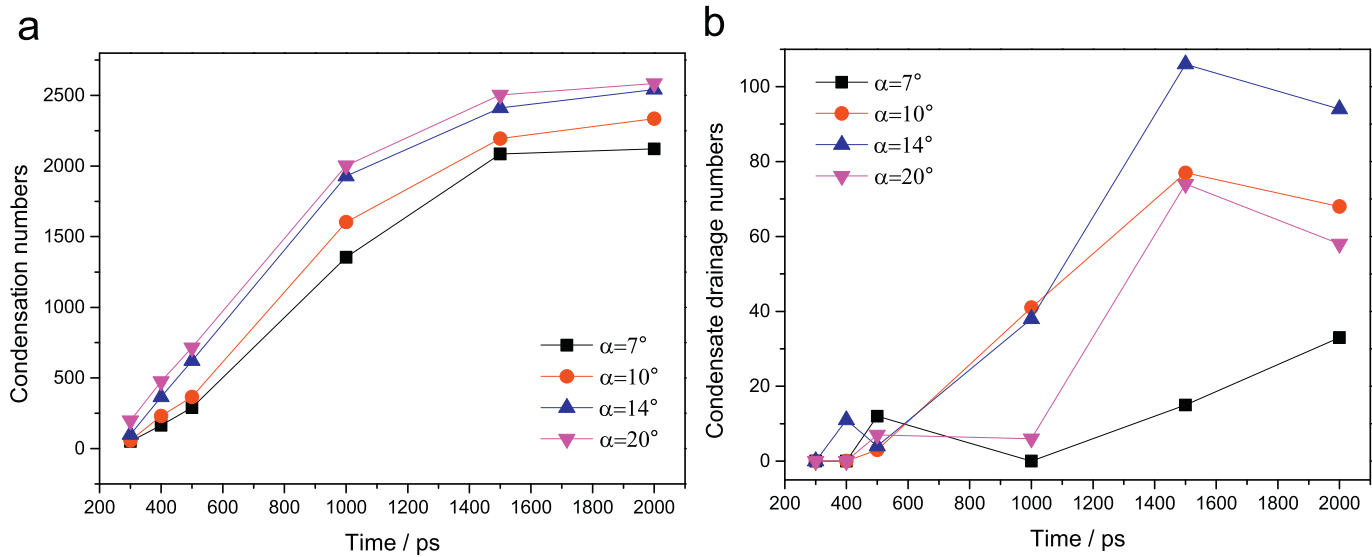


Fig. 8. Condensation numbers and condensate drainage numbers of water molecules at different vertex angles of Group B

didn't meet the coalesce condition and it took more time to enlarge the nucleus and nanoscale droplet to finish the final coalescence. In $\alpha = 14^\circ$, only one nucleus at the bottom survived and gobble up the other sub-clusters (Fig. 6p). Finally, it grew to a nanoscale droplet and the DWC firstly finished in $\alpha = 14^\circ$, indicating that condensation rate was larger and condensation process was quicker in this case. What's more, as two nuclei just finished gobbling up each other in $\alpha = 14^\circ$, the nanoscale droplet didn't have enough time to increase height leading to more spread areas of nanoscale droplet. Therefore, the droplet was flattest and narrowest in this case than other three cases, according well with results in Fig. 7. With time went on, the nucleus and nanoscale droplet in $\alpha = 7^\circ$ (Fig. 6e), $\alpha = 10^\circ$ (Fig. 6k) and $\alpha = 20^\circ$ (Fig. 6w) coalesced to each other and DWC appeared. As the hydrophilic surface in $\alpha = 7^\circ$ was smallest and condensation hardly happened on hydrophobic surface, the droplet in this case could only get higher and narrower to continue condensation (Fig. 6f), which obtained the largest $\bar{\delta}$ and smallest γ . In the end, droplet in $\alpha = 20^\circ$ was flattest and widest with largest wedge-shaped hydrophilic surface as shown in Fig. 7.

Compared the condensation of four different vertex angles in Group B, DWC finally happened in all cases. The condensation numbers and condensate drainage numbers of water molecules were recorded in Fig. 8. The larger hydrophilic surface attracted more water molecules, leading to the higher condensation numbers. However, the difference of condensation numbers between $\alpha = 14^\circ$ and $\alpha = 20^\circ$ was not big. In addition, the condensate drainage numbers in $\alpha = 14^\circ$ was much larger than other conditions, indicating that droplet in $\alpha = 14^\circ$ would move fastest towards the direction of bottom of wedge-shaped surface if the direction size was large enough. Too small wedge-shaped surface would take more time to form a main nucleus while too large wedge-shaped surface would form two main nuclei and it also would take more time for two nuclei to coalesce to form a nanoscale droplet. Hence, it can be concluded that the DWC rate was quicker and condensate drainage was better in $\alpha = 14^\circ$ in these four conditions.

The movement of nanoscale droplet on a composite wedge-shaped surface with multi-gradients was studied in our former work [9] and the schematic diagram of driving force of nanoscale droplet was shown in Fig. 9. The driven force along x direction (F_x) made the nanoscale droplet move towards the bottom of wedge-shaped surface, expressed as [9]:

$$F_x = F \times \sin\left(\frac{\alpha}{2}\right) = A \times \delta \times \sin\left(\frac{\alpha}{2}\right) \quad (5)$$

Where F was driven force generated by wettability gradient, δ was

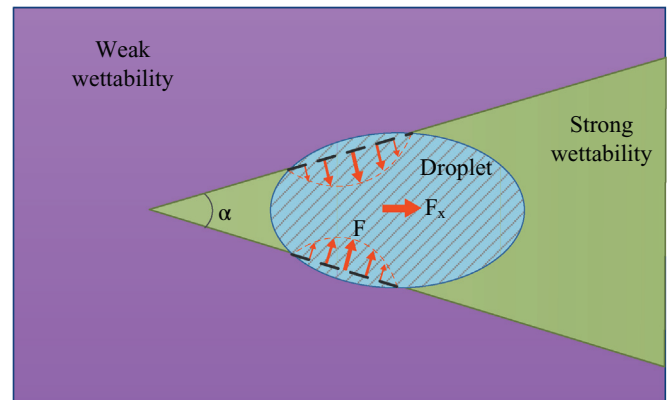


Fig. 9. Schematic diagram of driving force of nanoscale droplet

contact area of droplet on the boundary area of two different wettability surfaces, A was constant.

Smaller vertex angle would provide more contact area δ for droplet, indicating an inversely proportional between δ and α . As can be seen from Eq. (5), there was an inflection point when α increased from 0 to 180° . The larger F_x was more helpful to condensate drainage. Therefore, there would be a best vertex angle for condensate drainage and it was $\alpha = 14^\circ$ in this study, corresponding well with the discussion above.

4. Conclusions

The model of water vapor condensation on a composite wedge-shaped surface with multi wettability gradients was built and studied by molecular dynamics. The simulation results showed that FWC appeared in Group A and DWC formed in Group B. However, there was no condensation in Group C. Although the FWC in Group A could drain, the drainage rate was very slow. Only in Group B, the DWC could form water droplet and the movement of droplet could be controlled by the wedge-shaped surface, which was helpful for condensate drainage. When comparing the effect of different vertex angle, the smaller vertex angle could finish the FWC more quickly in Group A due to the smaller area of super hydrophilic surface. In group B, small wedge-shaped surface would take more time to form main nucleus, while large wedge-shaped surface forming two nuclei also took more time to form a whole droplet. In that case, it can be concluded that DWC rate was quicker and

condensation drainage was better in vertex angle of 14° in these four conditions. The composite wedge-shaped surface with multi wettability gradients could accelerate the condensate drainage and the vertex angle of 14° was the best condition, which will provide a microcosmic mechanism and support for macro experimental results.

Supplementary data to this article can be found online at <https://doi.org/10.1016/j.icheatmasstransfer.2019.03.011>.

Acknowledgment

This work was supported by International Cooperation Project of China Manned Space Program.

References

- [1] A.R. Parker, C.W. Lawrence, Water capture by a desert beetle, *Nature* 414 (2001) 33–34.
- [2] C. Luo, Theoretical exploration of barrel-shaped drops on cactus spines, *Langmuir* 31 (2015) 11809–11813.
- [3] J. Ju, H. Bai, Y. Zheng, T. Zhao, R. Fang, L. Jiang, A multi-structural and multi-functional integrated fog collection system in cactus, *Nat. Commun.* 3 (2012) 1247.
- [4] Y. Zheng, H. Bai, Z. Huang, X. Tian, F. Nie, Y. Zhao, J. Zhai, L. Jiang, Directional water collection on wetted spider silk, *Nature* 463 (2010) 640–643.
- [5] Y. Chen, Y. Zheng, Bioinspired micro-/nanostructure fibers with a water collecting property, *Nanoscale* 6 (2014) 7703–7714.
- [6] H. Gau, S. Herminghaus, P. Lenz, R. Lipowsky, Liquid morphologies on structured surfaces: from microchannels to microchips, *Science* 283 (1999) 46–49.
- [7] A.I. ElSherbini, A.M. Jacobi, A model for condensate retention on plain-fin heat exchangers, *J. Heat. Trans-T ASME* 128 (2005) 427–433.
- [8] S.A. Idem, A.M. Jacobi, V.W. Goldschmidt, Fin heat transfer modeling and its impact on predictions of efficiency and condensation in gas-fired boilers, *Heat. Transf. Eng.* 21 (2000) 7–18.
- [9] B. Xu, Z.Q. Chen, Droplet movement on a composite wedge-shaped surface with multi-gradients and different gravitational field by molecular dynamics, *Microgravity Sci. Tec.* 30 (2018) 571–579.
- [10] H.W. Hu, G.H. Tang, D. Niu, Experimental investigation of condensation heat transfer on hybrid wettability finned tube with large amount of noncondensable gas, *Int. J. Heat Mass Transf.* 85 (2015) 513–523.
- [11] N. Miljkovic, E.N. Wang, Condensation heat transfer on superhydrophobic surfaces, *MRS Bull.* 38 (2013) 397–406.
- [12] J. Cheng, A. Vandadi, C.L. Chen, Condensation heat transfer on two-tier superhydrophobic surfaces, *Appl. Phys. Lett.* 101 (2012) 131909.
- [13] T. Murase, H.S. Wang, J.W. Rose, Marangoni condensation of steam-ethanol mixtures on a horizontal tube, *Int. J. Heat Mass Transf.* 50 (2007) 3774–3779.
- [14] S. Lee, K. Cheng, V. Palme, M.M.H. Bhuiya, K.J. Kim, B.J. Zhang, H. Yoon, Heat transfer measurement during dropwise condensation using micro/nano-scale porous surface, *Int. J. Heat Mass Transf.* 65 (2013) 619–626.
- [15] X.M. Chen, J. Wu, R.Y. Ma, M. Hua, N. Koratkar, S.H. Yao, Z.K. Wang, Nanograss micropyramidal architectures for continuous dropwise condensation, *Adv. Funct. Mater.* 21 (2011) 4617–4623.
- [16] N. Miljkovic, R. Enright, Y. Nam, K. Lopez, N. Dou, J. Sack, E.N. Wang, Jumping-droplet-enhanced condensation on scalable superhydrophobic nanostructured surfaces, *Nano Lett.* 13 (2012) 179–187.
- [17] R.S. Subramanian, N. Moumen, J.B. McLaughlin, Motion of a drop on a solid surface due to a wettability gradient, *Langmuir* 21 (25) (2005) 11844–11849.
- [18] Y.F. Zheng, J. Cheng, C.L. Zhou, H.T. Xing, X.F. Wen, P.H. Pi, S.P. Xu, Droplet motion on a shape gradient surface, *Langmuir* 33 (17) (2017) 4172–4177.
- [19] M.M. Garimella, S. Koppu, S.S. Kadlaskar, V. Pillutla, Abhijeet and W. Choi, Difference in growth and coalescing patterns of droplets on bi-phobic surfaces with varying spatial distribution, *J. Colloid Interface Sci.* 505 (2017) 1065–1073.
- [20] B.L. Peng, X.H. Ma, Z. Lan, W. Xu, R.F. Wen, Experimental investigation on steam condensation heat transfer enhancement with vertically patterned hydrophobic-hydrophilic hybrid surfaces, *Int. J. Heat Mass Transf.* 83 (2015) 27–38.
- [21] T.Y. Song, Z. Lan, X.H. Ma, T. Bai, Molecular clustering physical model of steam condensation and the experimental study on the initial droplet size distribution, *Int. J. Therm. Sci.* 48 (2009) 2228–2236.
- [22] K. Yasuoka, M. Matsumoto, Molecular dynamics of homogeneous nucleation in the vapor phase I. Lennard-Jones fluid, *J. Chem. Phys.* 109 (1998) 8451–8462.
- [23] K. Yasuoka, M. Matsumoto, Molecular dynamics of homogeneous nucleation in the vapor phase II. Water, *J. Chem. Phys.* 109 (1998) 8463–8470.
- [24] J. Jung, E. Jang, M.A. Shoaib, K. Jo, J.S. Kim, Droplet formation and growth inside a polymer network: a molecular dynamics simulation study, *J. Chem. Phys.* 144 (2016) 134502.
- [25] P.R. Wolde, D. Frenkel, Computer simulation study of gas-liquid nucleation in a Lennard-Jones system, *J. Chem. Phys.* 109 (1998) 9901–9918.
- [26] J. Diemand, R. Angelil, K.K. Tanaka, H. Tanaka, Large scale molecular dynamics simulations of homogeneous nucleation, *J. Chem. Phys.* 139 (2013) 074309.
- [27] K. Yasuoka, G.T. Gao, X.C. Zeng, Molecular dynamics simulation of supersaturated vapor nucleation in slit pore, *J. Chem. Phys.* 112 (2000) 4279–4285.
- [28] S. Toxværd, Molecular dynamics simulation of heterogeneous nucleation at a structureless solid surface, *J. Chem. Phys.* 117 (2002) 10303–10310.
- [29] D. Niu, G.H. Tang, The effect of surface wettability on water vapor condensation in nanoscale, *Sci. Rep.-UK* 6 (2016) 19192.
- [30] W. Xu, Z. Lan, B.L. Peng, R.F. Wen, X.H. Ma, Effect of surface free energies on the heterogeneous nucleation of water droplet: a molecular dynamics simulation approach, *J. Chem. Phys.* 142 (5) (2017) 054701.
- [31] Q. Sheng, J. Sun, Q. Wang, W. Wang, H.S. Wang, On the onset of surface condensation: formation and transition mechanisms of condensation mode, *Sci. Rep.-UK* 6 (2016) 30764.
- [32] S. Plimpton, Fast parallel algorithms for short-range molecular dynamics, *J. Comput. Phys.* 117 (1) (1995) 1–19.
- [33] S.L. Price, A.J. Stone, M. Alderton, Explicit formulae for the electrostatic energy, forces and torques between a pair of molecules of arbitrary symmetry, *Mol. Phys.* 52 (4) (1984) 987–1001.
- [34] J. De Coninck, T.D. Blake, Wetting and molecular dynamics simulations of simple liquids, *Annu. Rev. Mater. Res.* 38 (2008) 1–22.
- [35] A. Hens, R. Agarwal, G. Biswas, Nanoscale study of boiling and evaporation in a liquid Ar film on a Pt heater using molecular dynamics simulation, *Int. J. Heat Mass Transf.* 71 (2014) 303–312.
- [36] T. Fu, Y. Mao, Y. Tang, Y. Zhang, W. Yuan, Molecular dynamics simulation on rapid boiling of thin water films on cone-shaped nanostructure surfaces, *Nanosc Microsc. Therm.* 19 (2015) 17–30.
- [37] H.R. Seyf, Y. Zhang, Effect of nanotextured array of conical features on explosive boiling over a flat substrate: a nonequilibrium molecular dynamics study, *Int. J. Heat Mass Transf.* 66 (2013) 613–624.
- [38] M. Barisik, A. Beskok, Boundary treatment effects on molecular dynamics simulations of interface thermal resistance, *J. Comput. Phys.* 231 (2012) 7881–7892.
- [39] A. Alexiadis, S. Kassinos, Molecular simulation of water in carbon nanotubes, *Chem. Rev.* 108 (2008) 5014–5034.
- [40] T. Koishi, K. Yasuoka, S. Fujikawa, T. Ebisuzaki, X.C. Zeng, Coexistence and transition between Cassie and Wenzel state on pillared hydrophobic surface, *PNAS* 106 (2009) 8435–8440.
- [41] F.H. Stillinger, Rigorous basis of the frenkel-band theory of association equilibrium, *J. Chem. Phys.* 38 (1963) 1486–1494.
- [42] A.C. Antony, T. Liang, S.B. Sinnott, Nanoscale structure and dynamics of water on Pt and Cu surfaces from MD simulations, *Langmuir* 34 (2018) 11905–11911.